On stochastic modeling of flow in multimodal heterogeneous formations

Zhiming Lu and Dongxiao Zhang

Hydrology, Geochemistry, and Geology Group (EES-6), Los Alamos National Laboratory, Los Alamos, New Mexico, USA

Received 22 October 2001; revised 29 April 2002; accepted 29 April 2002; published 11 October 2002.

[1] Most existing stochastic models are developed for unimodal porous media that may be well characterized with only the first two statistical moments. However, the distribution of hydraulic properties, such as hydraulic conductivity, may possess a multiplicity of modes; thus the first two moments may not be adequate to characterize properties of such porous media. In turn, the stochastic models developed for unimodal porous media may not be applicable to flow and transport in a multimodal heterogeneous porous medium. This study investigates under what circumstances the second-order moment-based stochastic models are applicable to multimodal heterogeneous porous media. We assume that a porous medium is composed of a number of materials (categories), each of which may have a different mean, variance, and correlation scale. The distribution of materials in the domain is characterized by indicator random variables. We first derive analytical expressions for the mean and covariance of the log saturated hydraulic conductivity ($\ln K_s$) of the multimodal porous medium in terms of categorical proportions, transition probability among categories, and covariances of indicator random variables. We express the covariance in terms of the statistics of materials in the porous medium, which allows us to accurately evaluate the variance and the correlation length of the composite $\ln K_s$ field. We then solve the second-order moment equations for the ''equivalent'' unimodal field with an exponential covariance with a single correlation scale computed for the composite field. On the other hand, we conduct two sets of Monte Carlo simulations: one with multimodal random fields, and the other with ''equivalent'' unimodal random fields. Examples for porous media with two materials are given. Numerical experiments show that a bimodal $\ln K_s$ field may be well approximated by an equivalent unimodal field when one of the two modes is dominant, under which condition the applicability of the second-order moment-based model is subject to the same limitation of relatively small variance as that for unimodal fields. When the bimodal distribution has two more or less equally important modes, although it cannot be adequately represented by an equivalent unimodal distribution, the second-order moment-based stochastic model seems to be applicable to systems with larger composite variances than it does for an one-mode-dominant distribution. *INDEX TERMS:* 1829 Hydrology: Groundwater hydrology; 1869 Hydrology: Stochastic processes; 3230 Mathematical Geophysics: Numerical solutions; *KEYWORDS:* stochastic, heterogeneity, bimodal, multimodal, multiscale

Citation: Lu, Z., and D. Zhang, On stochastic modeling of flow in multimodal heterogeneous formations, *Water Resour. Res.*, *38*(10), 1190, doi:10.1029/2001WR001026, 2002.

1. Introduction

[2] It is well known that geological formations are ubiquitously heterogeneous. Stochastic approaches to flow and transport in heterogeneous porous media have been extensively studied in the last two decades, and many stochastic models have been developed [e.g., *Dagan*, 1989; *Gelhar*, 1993; *Zhang*, 2002]. Most of these models, however, assume that the porous medium being studied can be characterized by the first two moments (mean and covariance) and the covariance can be described with one single correlation scale. Although some field studies [e.g., *Hoeksema and Kitanidis*, 1984; *Sudicky*, 1986; *Gelhar*, 1993] have shown that the hydraulic conductivity in some cases is unimodal and can be characterized by a spatial correlation structure defined by a covariance (or variogram) with a single, finite length scale; this in general may not be true. For example, in a sand-shale (or a fractured porous) formation, the hydraulic conductivity may have a large contrast between sand and shale (or fracture and matrix) and may thus exhibit a bimodal distribution. In a bimodal or more generally, multimodal medium, the first two moments are not adequate for describing its distribution. Hence, moment-based stochastic models developed for unimodal heterogeneous porous media may not be directly applicable to flow and transport in multimodal heterogeneous porous media. One

question we would like to ask is under what circumstances the moment-based stochastic models developed mainly for flow in the unimodal heterogeneous media can be applied directly to flow in the multimodal heterogeneous systems.

[3] A few studies have been conducted on flow and transport in a multimodal porous medium [*Desbarats*, 1987, 1990; *Rubin and Journel*, 1991; *Rubin*, 1995; *Russo et al.*, 2001]. *Desbarats* [1987, 1990] modeled the permeability of a sandstone reservoir as a bimodal attribute of two possible values, K_{ss} and K_{sh}, assuming that the discontinuous low-permeability shale streaks in the sandstone reservoir are the dominant source of heterogeneity and that the variation of permeability within the sandstone or shale is of secondary importance. Variations within sandstone or shale are ignored. *Rubin and Journel* [1991] decompose the random function of interest, say, $Z(x)$, into a series of indicator random functions, which allows assigning specific spatial structure to each class of Z values. The effect of bimodal heterogeneity on transport has been studied by *Rubin and Journel* [1991] and *Rubin* [1995]. Both assumed that the spatial distribution of $Z_1(x)$ and $Z_2(x)$ are independent of the indicator random variable and thus the spatial structures of Z_1, Z_2, and the indicator random variable can be assigned arbitrarily. *Russo et al.* [2001] investigated flow and transport of a tracer solute in variably saturated bimodal heterogeneous porous media and in the corresponding "equivalent" unimodal media. Again, the indicator random variable is modeled by assigning its own spatial structure, independent of the properties of the composite materials. It is known that the mean and variance of the indicator random variables are related to the volumetric proportion of each individual material. For a bimodal porous medium, for example, $\langle I_i(\mathbf{x})\rangle = p_i$ and $\sigma^2_{I_i} = p_1 p_2$, where p_i and $I_i(\mathbf{x})$ are the volumetric proportion of material i and its indicator random variable. Therefore, it may not be reasonable to assume that the correlation structures of the indicator variables can be assigned arbitrarily. Thus, the second question we would like to ask is how to quantitatively determine spatial structures of the indicator random variables based on the volumetric proportions and spatial structures of the materials.

[4] The Markov chain method has been applied to geological formations with different materials [*Krumbein*, 1968; *Krumbein and Dacey*, 1969; *Gingerich*, 1969; *Harbaugh and Bonham-Carter*, 1970; *Dacey and Krumbein*, 1970; *Miall*, 1973; *Agterberg*, 1974; *Ethier*, 1975; *Lin and Harbaugh*, 1984; *Rolke*, 1991; *Politis*, 1994; *Goovaerts*, 1994, 1996; *Carle*, 1996, 1997; *Carle and Fogg*, 1996, 1997; *Carle et al.*, 1998]. The distribution of materials is characterized by the transition probability between different materials. It has been shown [*Carle*, 1996; *Carle and Fogg*, 1997] that, in characterizing the structure of the indicator random variables, the transition probability between different categories is equivalent to the autocovariance of the indicator random variables and the former can be easily derived from field measurements.

[5] The aims of this study are (1) to derive explicit expressions for the covariance function of indicator random variables, based on properties of different materials and (2) to discuss the general requirements at which the second-order moment-based stochastic model with a covariance function of a single correlation length may be applied to a porous medium with multimodal heterogeneity.

2. Mean and Covariance of Multimodal Heterogeneous Fields

[6] Let $Y(\mathbf{x})$ be an attribute of interest, such as log hydraulic conductivity, and be expressed as

$$Y(\mathbf{x}) = \sum_{i=1}^{M} I_i(\mathbf{x}) Y_i(\mathbf{x}) \tag{1}$$

where $Y_i(\mathbf{x}), i = \overline{1, M}$, stands for the attribute $Y(\mathbf{x})$ of different materials (e.g., facies) at location $\mathbf{x}$, M is the number of categories (materials), and $I_i(\mathbf{x}), i = \overline{1, M}$, are indicator spatial random variables defined over a domain Ω as

$$I_i(\mathbf{X}) = \begin{cases} 1 \text{ if category i occurs at location } \mathbf{X} \\ 0 \text{ otherwise.} \end{cases} \tag{2}$$

For a continuous attribute $Y(\mathbf{x})$, $I_i(\mathbf{x})$ can be defined using a set of different cutoffs [*Deutsch and Journel*, 1992; *Rubin and Journel*, 1991]. It is clear that $\Sigma_i I_i(\mathbf{x}) = 1$, for any $\mathbf{x} \in \Omega$. By definition, the joint probability of $I_i(\mathbf{x})$ and $I_j(\chi)$ can be expressed as

$$p_{ij}(\mathbf{X}, \chi) = Pr\{I_i(\mathbf{X}) = 1, I_j(\chi) = 1\} = E\{I_i(\mathbf{X}) I_j(\chi)\} \tag{3}$$

and their marginal probability as

$$\begin{aligned} p_i(\mathbf{X}) &= Pr\{I_i(\mathbf{X}) = 1\} = E\{I_i(\mathbf{X})\} \\ p_j(\chi) &= Pr\{I_j(\chi) = 1\} = E\{I_j(\chi)\}. \end{aligned} \tag{4}$$

The transition probability $t_{ij}(\mathbf{x}, \chi)$ is defined as the probability of category j occurring at location χ, given the condition that category i occurs at location $\mathbf{x}$:

$$t_{ij}(\mathbf{x}, \chi) = Pr\{I_j(\chi) = 1 | I_i(\mathbf{x}) = 1\} = E\{I_i(\mathbf{x}) I_j(\chi)\} / p_i(\mathbf{x}). \tag{5}$$

The covariance of the indicator variables can be given as

$$C_{I,ij}(\mathbf{x}, \chi) = E\{I_i(\mathbf{x}) I_j(\chi)\} - E\{I_i(\mathbf{x})\} E\{I_j(\chi)\}. \tag{6}$$

Substituting (3)–(5) into (6), the covariance of indicator random variables can be expressed in terms of categorical proportions and transitionprobability t_{ij}

$$C_{I,ij}(\mathbf{x}, \chi) = [t_{ij}(\mathbf{x}, \chi) - p_j(\chi)] p_i(\mathbf{x}). \tag{7}$$

It should be noted that, since $t_{ij}(\mathbf{x}, \chi) p_i(\mathbf{x}) = t_{ji}(\chi, \mathbf{x}) p_j(\chi)$, the covariances of the indicator variables are symmetric with respect to locations $\mathbf{x}$ and χ, but the transition probability $t_{ij}(\mathbf{x}, \chi)$ in general is not symmetric with respect to its indexes i and j.

[7] It has been argued [*Rubin and Journel*, 1991; *Rubin*, 1995] that I_i and Y_j are mutually uncorrelated. Under this condition, the mean and covariance of Y can be derived as

$$\langle Y(\mathbf{x}) \rangle = \sum_{i=1}^{M} E\{I_i(\mathbf{x})\} E\{Y_i(\mathbf{x})\} = \sum_{i=1}^{M} p_i(\mathbf{x}) \langle Y_i(\mathbf{x}) \rangle \tag{8}$$

$$C_Y(\mathbf{x},\boldsymbol{\chi}) = E\{[Y(\mathbf{x}) - \langle Y(\mathbf{x})\rangle][Y(\boldsymbol{\chi}) - \langle Y(\boldsymbol{\chi})\rangle]\}$$
$$= \sum_{i,j=1}^{M} t_{ij}(\mathbf{x},\boldsymbol{\chi}) p_i(\mathbf{x}) C_{Y,ij}(\mathbf{x},\boldsymbol{\chi}) + \sum_{i,j=1}^{M} \{t_{ij}(\mathbf{x},\boldsymbol{\chi}) - p_j(\boldsymbol{\chi})\} p_i(\mathbf{x}) \langle Y_i(\mathbf{x})\rangle \langle Y_j(\boldsymbol{\chi})\rangle, \quad (9)$$

or, in terms of the covariance of indicator random variables, (9) becomes

$$C_Y(\mathbf{x},\boldsymbol{\chi}) = \sum_{i,j=1}^{M} [C_{I,ij}(\mathbf{x},\boldsymbol{\chi}) + p_i(\mathbf{x}) p_j(\boldsymbol{\chi})] C_{Y,ij}(\mathbf{x},\boldsymbol{\chi}) + \sum_{i,j=1}^{M} C_{I,ij}(\mathbf{x},\boldsymbol{\chi}) \langle Y_i(\mathbf{x})\rangle \langle Y_j(\boldsymbol{\chi})\rangle. \quad (10)$$

In particular, because $t_{ij}(\mathbf{x}, \mathbf{x}) = \delta_{ij}$, the variance of log hydraulic conductivity can be derived from (9) as

$$\sigma_Y^2(\mathbf{x}) = \sum_{i=1}^{M} p_i(\mathbf{x}) \sigma_{Y_i}^2(\mathbf{x}) + \sum_{i=1}^{M} p_i(\mathbf{x}) \langle Y_i(\mathbf{x})\rangle^2 - \sum_{i,j=1}^{M} p_i(\mathbf{x}) p_j(\mathbf{x}) \langle Y_i(\mathbf{x})\rangle \langle Y_j(\mathbf{x})\rangle. \quad (11)$$

For second-order stationary media for which $p_i(\mathbf{x}) = const$, $\langle Y_i(\mathbf{x})\rangle = const$, $C_Y(\mathbf{x},\boldsymbol{\chi}) = C_Y(\mathbf{x}-\boldsymbol{\chi})$, and $t_{ij}(\mathbf{x},\boldsymbol{\chi}) = t_{ij}(\mathbf{x}-\boldsymbol{\chi})$, we have

$$C_{I,ij}(h) = [t_{ij}(h) - p_j] p_i \quad (12)$$

$$\langle Y\rangle = \sum_{i=1}^{M} p_i \langle Y_i\rangle \quad (13)$$

$$C_Y(h) = \sum_{i,j=1}^{M} [C_{I,ij}(h) + p_i p_j] C_{Y,ij}(h) + \sum_{i,j=1}^{M} C_{I,ij}(h) \langle Y_i\rangle \langle Y_j\rangle \quad (14)$$

$$\sigma_Y^2 = \sum_{i=1}^{M} p_i \sigma_{Y_i}^2 + \sum_{i=1}^{M} p_i \langle Y_i\rangle^2 - \sum_{i,j=1}^{M} p_i p_j \langle Y_i\rangle \langle Y_j\rangle \quad (15)$$

where h is the separation distance. For statistically anisotropic media, h should be replaced by a separation vector. In the case of $M = 2$, (13)–(15) simplifies to well known expressions for bimodal porous media [*Desbarats*, 1990; *Rubin*, 1995; *Winter and Tartakovsky*, 2000; *Zhang*, 2002, pp. 73–76].

3. Covariance of Indicator Random Functions

[8] In the last section, we expressed the covariance of the composite log hydraulic conductivity field in terms of covariance functions of the indicator random variables. It is commonly assumed in the literature that the correlation structures of the indicator random variables are independent of each individual category [*Rubin and Journel*, 1991; *Rubin*, 1995; *Russo et al.*, 2001]. In this section, we derive expressions for the covariance of indicator random variables using the Markov chain approach, based on the statistics of different materials in a porous medium.

[9] It is assumed in a three-dimensional Markov chain model that spatial variability in any direction can be characterized by a one-dimensional Markov chain model [*Lin and Harbaugh*, 1984; *Politis*, 1994]. For a one-dimensional Markov chain model, the continuous-lag transition probability matrix $\mathbf{T}$ for any lag h can be written as [*Carle*, 1996; *Carle and Fogg*, 1997]:

$$\mathbf{T}(h) = e^{\mathbf{R}h} \quad (16)$$

where $\mathbf{R}$ is an $M \times M$ transition rate matrix whose entry r_{ij} represents the rate of change from category i to category j per unit length of category i in the given direction. If the transition rate matrix $\mathbf{R}$ is known, the transition probability matrix $\mathbf{T}$ can be evaluated by an eigenvalue analysis. Let η_i, $i = \overline{1, M}$, be eigenvalues of the transition rate matrix $\mathbf{R}$ and $\mathbf{Z}_i$, $i = \overline{1, M}$, be their corresponding spectral component matrixes that are evaluated by

$$\mathbf{Z}_i = \prod_{m \neq i} (\eta_m \mathbf{E} - \mathbf{R}) / \prod_{m \neq i} (\eta_m - \eta_i) \quad (17)$$

where $\mathbf{E}$ is the identical matrix, (16) then becomes

$$\mathbf{T}(h) = \sum_{i=1}^{M} e^{\eta_i h} \mathbf{Z}_i, \quad (18)$$

which means that the transition probability is the summation of a series of exponential terms. By recalling (12), (18) implies that the covariance of indicator random functions is a summation of exponential terms.

[10] Now we focus on how to evaluate $\mathbf{R}$ and relate the covariances of indicator random variables to the statistics of different materials in the porous medium. If we have a transition probability matrix $\mathbf{T} = (t_{ij})$ measured at a discrete lag Δh in a direction ϕ, the transition rate matrix $\mathbf{R}_\phi$ can be computed [*Agterberg*, 1974; *Carle*, 1996; *Carle and Fogg*, 1997]

$$\mathbf{R}_\phi = \frac{\ln(\mathbf{T}(\Delta h_\phi))}{\Delta h_\phi} \quad (19)$$

which again involves an eigenvalue analysis. In this case, the transition probability matrix for the direction ϕ at any lag can be calculated using (16) to (18), and the proportions of all categories can be calculated by multiplying the transition matrix to itself a number of times until the product is stablized.

[11] In reality, discrete lag transition probability matrix in the vertical direction may be obtained from, for example, borehole data. Thus transition rate matrix can be computed using (19). However, in the lateral directions, sparse data may prevent directly measuring the discrete lag transition probability matrix. In this case, one is unable to calculate $\mathbf{R}$ using (19); thus, some alternative ways for deriving $\mathbf{R}$ are needed.

[12] Taking the derivative of (16) and letting $h = 0$, we have [*Ross*, 1993; *Carle and Fogg*, 1997]

$$\mathbf{R} = \left.\frac{d\mathbf{T}(h)}{dh}\right|_{h=0}. \quad (20)$$

Because the transition probability t_{ij} has to satisfy the following equations:

$$\sum_{j=1}^{M} t_{ij} = 1 \qquad i = \overline{1,M} \tag{21}$$

$$\sum_{i=1}^{M} p_i t_{ij} = p_j \qquad j = \overline{1,M}, \tag{22}$$

it follows immediately that transition rates r_{ij} satisfy [*Ross*, 1993; *Carle and Fogg*, 1997]

$$\sum_{j=1}^{M} r_{ij} = 0 \qquad i = \overline{1,M} \tag{23}$$

$$\sum_{i=1}^{M} p_i r_{ij} = 0 \qquad j = \overline{1,M}. \tag{24}$$

Equations (23) and (24) imply that $det(\mathbf{R}) = 0$; therefore, one of the eigenvalues of $\mathbf{R}$, say η_1, must be zero. The spectral component matrix $\mathbf{Z}_1$ corresponding to this zero eigenvalue has special meaning, i.e., any row of $\mathbf{Z}_1$ represents the proportions of all categories,

$$\mathbf{Z}_1 = \begin{bmatrix} p_1 & p_2 & \cdots & p_M \\ p_1 & p_2 & \cdots & p_M \\ & & \cdots & \\ p_1 & p_2 & \cdots & p_M \end{bmatrix}. \tag{25}$$

Equations (23) and (24) give $2M - 1$ independent equations, because one of the $2M$ equations can be derived from other $2M - 1$ equations. More equations are needed for solving $\mathbf{R}$.

[13] For a given porous medium, proportions of categories are the same in any direction. Therefore, once the transition matrix $\mathbf{T}$ (and so $\mathbf{R}$) in one direction ϕ_0 is known, $\mathbf{R}$ in any other direction ϕ can be estimated with some additional information. *Carle* [1996] shows that the diagonal terms of the transition rate matrix $\mathbf{R}_\phi$ is related to mean lengths:

$$r_{ii,\phi} = -\frac{1}{L_{i,\phi}} \qquad i = \overline{1,M}. \tag{26}$$

In practice, if the mean length of one category, say $L_{1,\phi}$, in direction ϕ is known, the mean lengths for all other categories in this direction can be calculated from $L_{i,\phi} = p_i L_{1,\phi}/p_1,\ i = \overline{1,M}$.

[14] For a bimodal porous medium, either knowing proportions and one mean length in the direction ϕ, or knowing two mean lengths in this direction is enough for solving $\mathbf{R}$ (see Appendix A), and the transition probability t_{ij} can be written as

$$t_{ij}(h) = p_j + \left(\delta_{ij} - p_j\right) e^{-h/\lambda_I} \tag{27}$$

where λ_I is defined as

$$\lambda_I = p_1 L_2 = p_2 L_1 = L_1 L_2/(L_1 + L_2), \tag{28}$$

which is the harmonic mean of the two mean lengths in the given direction. Substituting (27) into (12), one obtains the covariance of the indicator random variables:

$$C_{I,ij}(h) = p_i\left(\delta_{ij} - p_j\right) e^{-h/\lambda_I}. \tag{29}$$

Because of the constraint $I_1(\mathbf{x}) = 1 - I_2(\mathbf{x})$, the tensor $\mathbf{C}_I$ is symmetric and also $C_{I,11}(h) = C_{I,22}(h)$. It is seen from (29) that λ_I defined in (28) is in fact the correlation length of the indicator random variable. It should be emphasized that if the mean lengths of the materials are direction-dependent, the correlation length λ_I is also direction-dependent. For a stationary field, because the categorical proportions in all directions are the same, the isotropic ratio of the indicator random variable between any two directions equals the ratio of mean lengths of the any category in these two directions, i.e., $\lambda_I^{(1)}/\lambda_I^{(2)} = L_1^{(1)}/L_1^{(2)} = L_2^{(1)}/L_2^{(2)}$.

[15] For a porous medium with three materials, the transition probability can be written as (Appendix B)

$$t_{ij}(h) = p_j + \frac{e^{\eta_2 h}}{\eta_2 - \eta_3}\left[\eta_3\left(p_j - \delta_{ij}\right) + r_{ij}\right] + \frac{e^{\eta_3 h}}{\eta_3 - \eta_2}\left[\eta_2\left(p_j - \delta_{ij}\right) + r_{ij}\right] \tag{30}$$

where η_2 and η_3, given in Appendix B, are two nonzero (negative) eigenvalues of the transition rate matrix $\mathbf{R} = (r_{ij})$ (see Appendix B). Substituting (30) into (12) gives the covariance function of the indicator random variables as

$$C_{I,ij}(h) = \frac{p_i e^{\eta_2 h}}{\eta_2 - \eta_3}\left[\eta_3\left(p_j - \delta_{ij}\right) + r_{ij}\right] + \frac{p_i e^{\eta_3 h}}{\eta_3 - \eta_2}\left[\eta_2\left(p_j - \delta_{ij}\right) + r_{ij}\right]. \tag{31}$$

Once the covariances of the indicator random variables $C_{I,ij}(h)$ are known, $C_Y(h)$ can be calculated using (14), and the integral scale of the Y field can be derived by integrating $C_Y(h)$.

4. Bimodal Media

[16] We now concentrate on media with two materials: Y_1 and Y_2. Assuming independence between $Y_1(\mathbf{x})$ and $Y_2(\mathbf{x})$ and an exponential covariance function for each $Y_i(\mathbf{x})$,

$$C_{Y_i}(h) = \sigma_{Y_i}^2 e^{-\frac{h}{\lambda_i}} \qquad i = 1,2 \tag{32}$$

and substituting (29) and (32) into (14), one obtains

$$C_Y(h) = p_1^2\sigma_{Y_1}^2 e^{-\frac{h}{\lambda_1}} + p_2^2\sigma_{Y_2}^2 e^{-\frac{h}{\lambda_2}} + p_1 p_2(\langle Y_1\rangle - \langle Y_2\rangle)^2 e^{-\frac{h}{\lambda_I}} + p_1 p_2 e^{-\frac{h}{\lambda_I}}\left(\sigma_{Y_1}^2 e^{-\frac{h}{\lambda_1}} + \sigma_{Y_2}^2 e^{-\frac{h}{\lambda_2}}\right). \tag{33}$$

In (33), $p_1 + p_2 = 1$, σ_1^2 and λ_1 are the respective variance and correlation length of $Y_1(\mathbf{x})$, σ_2^2 and λ_2 are the respective

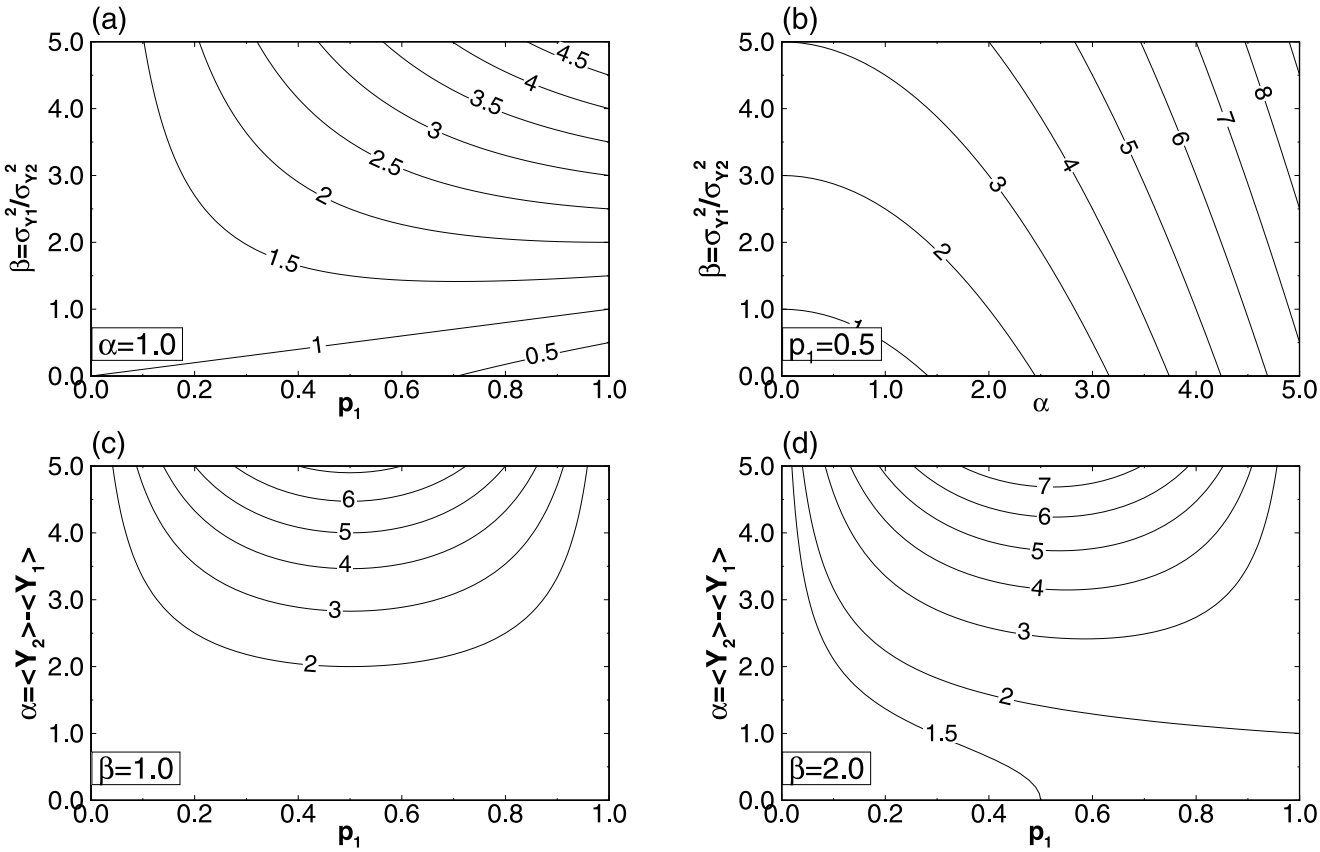

Figure 1. Variance of the composite log hydraulic conductivity as a function of proportions of materials, the contrast between materials, and variations in each material.

variance and correlation length of $Y_2(\mathbf{x})$, and λ_I is the correlation length of the geometry indicator. It is seen from (28) that $\lambda_I = p_2L_1 = p_1L_2$, where L_1 and L_2 are the mean lengths of materials 1 and 2, respectively. From (33), $C_Y(h)$ is the summation of five parts. The first two terms in (33) are contributions from materials 1 and 2, respectively; the third term is the contribution due to the geometry indicator random variable; and the last two terms are contributions due to the combination of the statistics of different materials and the spatial distribution of two materials (controlled by the indicator random variable). *Rubin* [1995] and *Russo et al.* [2001] have expressions similar to (33), but the major difference is that instead of assigning arbitrary correlation structure to the indicator variable, we expressed it explicitly as the harmonic mean of mean lengths of the two materials.

[17] The variance of $Y(\mathbf{x})$ can be obtained by setting $h = 0$ in (33)

$$\sigma_Y^2 = p_1\sigma_{Y_1}^2 + p_2\sigma_{Y_2}^2 + p_1p_2(\langle Y_1\rangle - \langle Y_2\rangle)^2. \tag{34}$$

Figure 1 shows the variance of the log hydraulic conductivity $Y(\mathbf{x})$ varying with parameters p_1, $\beta = \sigma_{Y_1}^2/\sigma_{Y_2}^2$, and the contrast of the mean $Y(\mathbf{x})$ between two materials, $\alpha = \langle Y_2\rangle - \langle Y_1\rangle$. Given $\alpha = 1.0$ and $\sigma_{Y_2}^2 = 1.0$, at $p_1 = 0.0$, the bimodal system degenerates to a unimodal system and the variance $\sigma_Y^2 = \sigma_{Y_2}^2 = 1.0$ (Figure 1a). When $p_1 = 1.0$, the medium becomes unimodal and its variance depends solely on $\sigma_{Y_1}^2$. For a small p_1, an increase of $\sigma_{Y_1}^2$ (i.e., increase of β, for the fixed $\sigma_{Y_2}^2$) has a little effect on the total σ_Y^2. For fixed proportions (Figure 1b), an increase in both α or β increases σ_Y^2; however, it seems that the increase of the contrast between two materials α has a relatively larger effect on the total heterogeneity σ_Y^2. Figure 1c illustrates the effect of proportion p_1 and α on σ_Y^2 for given $\beta = 1.0$. Certainly, when one material in the field is dominant (i.e., a small p_1 or large p_1), the contrast in the mean $Y(\mathbf{x})$ between two materials does not have a great effect on the total σ_Y^2 because the third term in (34) is relatively small due to a small p_1p_2. The curves in Figure 1c are symmetric with respect to proportion $p_1 = 0.5$. However, when $\beta \neq 1$ this symmetry does not exist. Figure 1d depicts the effect of proportion p_1 and α for a fixed $\beta = 2.0$.

[18] To investigate the effect of heterogeneity of each individual material on the total heterogeneity, we plot σ_Y^2 against p_1 for different values of α, β, and $\sigma_{Y_2}^2$ (Figure 2). Figure 2a shows the dependency of σ_Y^2 on α for given $\sigma_{Y_1}^2 = \sigma_{Y_2}^2$; Figure 2b illustrates the similar cases as in Figure 2a but with different β values for given $\sigma_{Y_2}^2 = 1$. It is clear from Figures 2a and 2b that, for a relatively large contrast in the mean log hydraulic conductivity between two materials, the contribution of the heterogeneity in each individual material to the total heterogeneity is less important. This confirms *Desbarats'* [1987] claim that the variation of permeability within sandstone or shale is of secondary importance because of the large contrast between sandstone and shale.

[19] Although $I(\mathbf{x})(=I_1(\mathbf{x}))$, $Y_1(\mathbf{x})$ and $Y_2(\mathbf{x})$ are assumed to be mutually uncorrelated (in the sense that given $I(\mathbf{x}) = 1$,

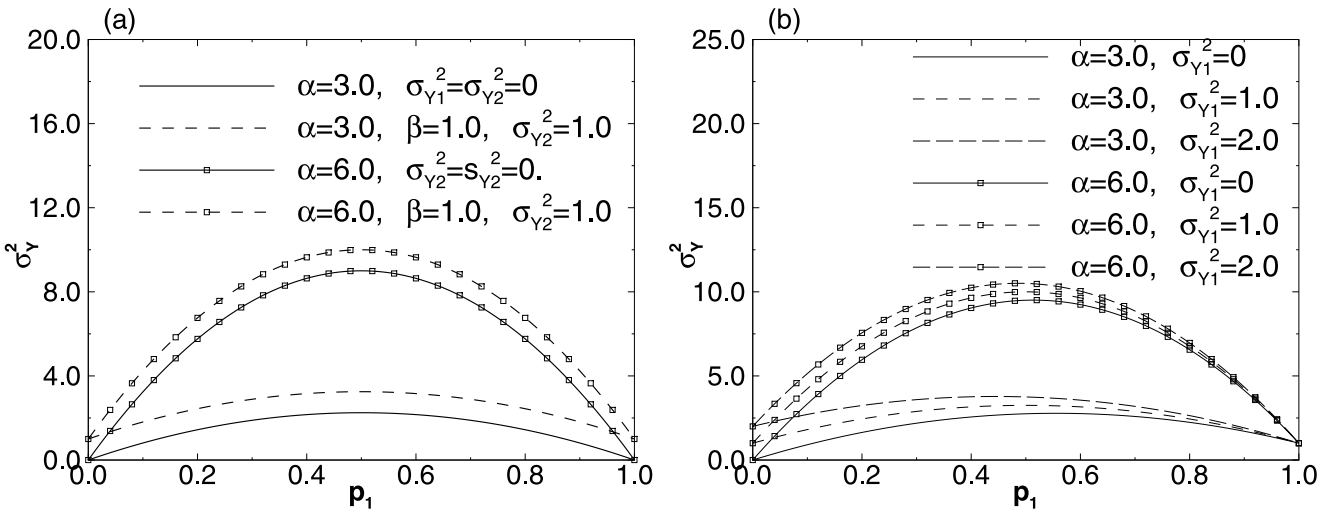

Figure 2. The effect of heterogeneity of each individual material on the total heterogeneity.

the value of $Y_1(\mathbf{x})$ is independent of $I(\mathbf{x})$), the correlation lengths λ_1 and λ_2 of $Y_1(\mathbf{x})$ and $Y_2(\mathbf{x})$ are not truly unrelated to λ_I of I. This is because the correlation length λ_1 is constrained by the geometry of facies $I_1(\mathbf{x}) = 1$, e.g., through its mean length L_1. Intuitively, the correlation length of each category depends on its mean length, and the category with the smaller mean length may have a smaller correlation length. It is reasonable to expect the range l_1 of the log hydraulic conductivity $Y_1(\mathbf{x})$ not to exceed the facies geometrical mean length L_1, i.e., $l_1 \leq L_1$. For an exponential covariance, one usually has $l_1 = 3\lambda_1$ and thus $3\lambda_1 = l_1 \leq L_1 = \lambda_I/p_2$. In turn, one has

$$\lambda_1 \leq \frac{\lambda_I}{3(1-p_1)}. \tag{35}$$

Similarly, for facies $I_2(\mathbf{x}) = 1$,

$$\lambda_2 \leq \frac{\lambda_I}{3(1-p_2)}. \tag{36}$$

which are consistent with that of *Ritzi* [2000, Table 1]. Equations (35) and (36) imply that, in numerical simulations of flow and transport in a bimodal heterogeneous porous medium, the correlation lengths of $Y_1(\mathbf{x})$, $Y_2(\mathbf{x})$, and the indicator variable I should not be assigned independently, without any constraints. While (35)–(36) estimate the maximum correlation lengths that the attribute $Y_1(\mathbf{x})$ and $Y_2(\mathbf{x})$ may attain, the actual values of λ_1 and λ_2 depend on the actual random fields, $Y_1(\mathbf{x})$ and $Y_2(\mathbf{x})$. The maximum correlation lengths for $Y_1(\mathbf{x})$ and $Y_2(\mathbf{x})$ as functions of the proportion p_1 are illustrated in Figure 3, which shows that the correlation length of each category may be either smaller or larger than the correlation length of the indicator variable, depending on its proportion. For example, if $p_1 = 0.2$ and $L_1 = 1.5$, one has $L_2 = p_2L_1/p_1 = 6.0$, $\lambda_I = p_1L_2 = p_2L_1 = 1.2$, $\lambda_1 \leq 0.5$ and $\lambda_2 \leq 2.0$. The integral scale of $Y(\mathbf{x})$ can be derived by integrating (33)

$$\lambda_Y = \frac{1}{\sigma_Y^2}\int_0^\infty C_Y(h)dh = \frac{p_1^2\sigma_{Y_1}^2\lambda_1 + p_2^2\sigma_{Y_2}^2\lambda_2 + p_1p_2(\langle Y_1\rangle - \langle Y_2\rangle)^2\lambda_I + p_1p_2\sigma_{Y_1}^2\frac{\lambda_1\lambda_I}{\lambda_1+\lambda_I} + p_1p_2\sigma_{Y_2}^2\frac{\lambda_2\lambda_I}{\lambda_2+\lambda_I}}{p_1\sigma_{Y_1}^2 + p_2\sigma_{Y_2}^2 + p_1p_2(\langle Y_1\rangle - \langle Y_2\rangle)^2}. \tag{37}$$

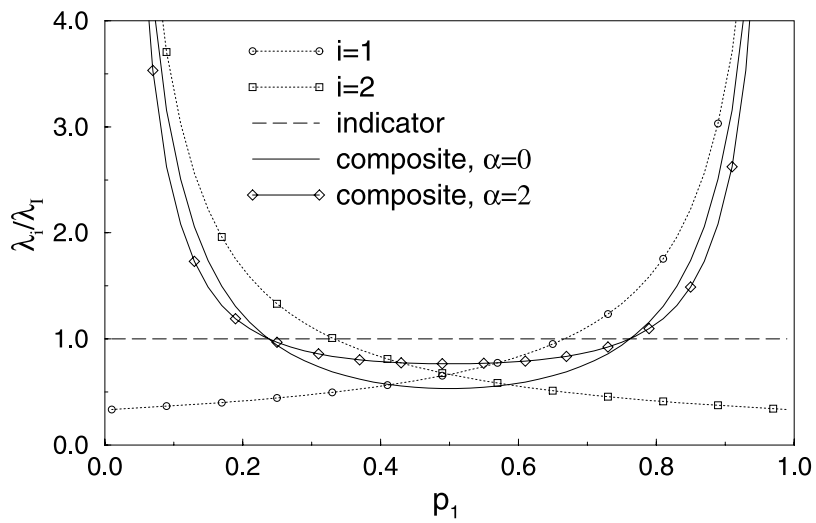

Figure 3. Maximum correlations length for each material as a function of proportion p_1.

Table 1. Statistical Parameters for All Illustrative Examples

	p_1	p_2	$\langle Y_1 \rangle$	$\langle Y_2 \rangle$	$\sigma^2_{Y_1}$	$\sigma^2_{Y_2}$	λ_i	λ_I	$\langle Y \rangle$	σ^2_Y	λ_Y
Case 1	0.3	0.7	−1.4	0.6	0.1	0.1	1.2	2.52	0.0	0.94	2.362
Case 2	0.3	0.7	−2.8	1.2	0.1	0.1	1.2	2.52	0.0	3.46	2.477
Case 3	0.3	0.7	−1.4	0.6	2.0	2.0	1.2	2.52	0.0	2.84	1.476
Case 4	0.3	0.7	−2.8	1.2	2.0	2.0	1.2	2.52	0.0	5.36	1.967
Case 5	0.5	0.5	−1.0	1.0	0.1	0.1	1.2	1.80	0.0	1.10	1.724
Case 6	0.5	0.5	−2.0	2.0	0.1	0.1	1.2	1.80	0.0	4.10	1.780
Case 7	0.5	0.5	−1.0	1.0	0.1	2.0	1.2	1.80	0.0	2.05	1.370
Case 8	0.5	0.5	−2.0	2.0	0.1	2.0	1.2	1.80	0.0	5.05	1.625
Case 9	0.5	0.5	−1.0	1.0	2.0	2.0	1.2	1.80	0.0	3.00	1.240
Case 10	0.5	0.5	−2.0	2.0	2.0	2.0	1.2	1.80	0.0	6.00	1.520
Case 11	0.5	0.5	−3.0	3.0	2.0	2.0	1.2	1.80	0.0	11.00	1.647

The dependency of the integral scale of the composite log hydraulic conductivity field λ_Y is also illustrated in Figure 3 for $\sigma^2_{Y_1} = \sigma^2_{Y_2} = 1$ and two different values of $\alpha = \langle Y_1 \rangle - \langle Y_2 \rangle$. It is seen from Figure 3 that the integral scale of the composite log hydraulic conductivity field λ_Y may be larger or smaller than λ_I, depending on p_1 and α.

5. Numerical Implementation

[20] To investigate the applicability of the second-order moment-based stochastic model with a single correlation length to a multimodal system, we illustrate a few examples for flow in a two-dimensional horizontal saturated porous medium with two materials. The domain of 12 $m \times 12$ m is uniformly discretized into 60 × 60 square elements with a size of 0.2 $m \times 0.2$ m. Three factors have been considered in material specifications in case design: the volumetric fractions of two materials; the contrast of the mean log hydraulic conductivity $Y(\mathbf{x}) = \ln K_s(\mathbf{x})$ between two materials; and the variability of $Y(\mathbf{x})$ within each material. Detailed specifications for materials in each case are listed in Table 1, where p_1 and p_2 are the fractions of two materials; $\langle Y_1 \rangle$ and $\langle Y_2 \rangle$ are their mean log hydraulic conductivities; and $\sigma^2_{Y_i}$ and λ_i are the variance and the correlation length for the ith material. The values of $\langle Y_1 \rangle$ and $\langle Y_2 \rangle$ are chosen such that the weighted mean $Y(\mathbf{x})$ for the composite field is zero. The parameters in the last three columns of Table 1, $\langle Y \rangle$, σ^2_Y, and λ_Y, are the respective (weighted) means, variances and correlation lengths of the composite fields that are calculated using (13), (34), and (37). These three parameters are called "equivalent" parameters and used later to define the "equivalent" unimodal porous medium.

[21] In all cases, the left and right boundaries are prescribed as constant hydraulic head of 10.5 m and 10.0 m, respectively, and the lateral are prescribed as no-flow boundaries. This produces a mean flow from the left to the right.

[22] Cases 1–4 ($p_1 = 0.3$) are designed against cases 5–10 ($p_1 = 0.5$) to examine the effects of categorical proportions and the symmetry of the Y distribution. The pair of case 2k-1 and case 2k ($k = \overline{1,5}$) is compared with each other to explore the effect of the contrast of the mean $Y(\mathbf{x})$ between the two materials. The effect of heterogeneity within each individual material is also examined by comparing case 1 versus case 3 (and also case 2 versus case 4, case 5 versus case 7 and case 9, case 6 versus case 8 and case 10). Cases 7 and 8 have volumetric fractions $p_1 = p_2 = 0.5$ but with an asymmetric Y distribution due to different degrees of heterogeneity within the two materials.

[23] For each case, we conducted two sets of Monte Carlo simulations and compared their results against those from the second-order moment-based stochastic models [*Zhang and Winter*, 1998; *Zhang and Lu*, 2002]. The second-order moment-based models are developed by first deriving equations governing the first two statistical moments of flow quantities with the technique of perturbation expansions and then solving these moment equations numerically. The results from these models are directly the first two moments of the flow quantity of interest. Because the moment equations are solved numerically, this approach can handle any arbitrarily complex covariance functions as well as flow nonstationarity caused by the presence of medium nonstationarity or finite flow boundaries. The details of this approach can be found in the works of *Zhang and Winter* [1998], *Zhang and Lu* [2002], or *Zhang* [2002].

[24] The first set of Monte Carlo simulations was performed for flow in a porous medium with two materials. For this purpose, similar to the two-stage procedure [*Deutsch and Journel*, 1992] we first generated 5000 two-dimensional 61 × 61 ($Y(\mathbf{x})$ is defined at nodes) Markovian random fields of two categories with given mean lengths $L_1 = 3.6$ m and $L_2 = p_2 L_1 / p_1$, using Transition Probability Geostatistical Software (T-PROGS) [*Carle et al.*, 1997]. We then generated 10,000 two-dimensional 61 × 61 unconditional Gaussian realizations with zero mean, unit variance, and a correlation length $\lambda_i = 1.20$ m (assuming the same correlation length for both materials, i.e., $\lambda_1 = \lambda_2$), using a sequential Gaussian random field generator *sgsim* from GSLIB [*Deutsch and Journel*, 1992]. The quality of the generated Markovian random fields was first checked by comparing their ensemble mean and variance with the specified mean and variance, i.e., $\langle I(\mathbf{x}) \rangle = \langle I_1(\mathbf{x}) \rangle = p_1 = L_1/(L_1 + L_2)$ and $\sigma^2_I(\mathbf{x}) = p_1 p_2 = L_1 L_2/(L_1 + L_2)^2$. The variogram calculated from the generated Markovian realizations was compared with the analytical, exponential model $\gamma(h) = \sigma^2_I\,[1.0 - \exp(-h/\lambda_I)]$ (Figures 4a–4d), where $\lambda_I = L_1 L_2/(L_1 + L_2)$. The quality of the generated Gaussian realizations has also been checked in a similar manner. All these comparisons indicate that both Gaussian realizations and Markovian realizations satisfy the specified mean, variance, and correlation length very well. In generating these Markovian realizations, the correlation length λ_I is not independently given but determined with the mean lengths for two materials specified. The correlation lengths λ_1 and λ_2 of log hydraulic conductivities Y_1 and Y_2

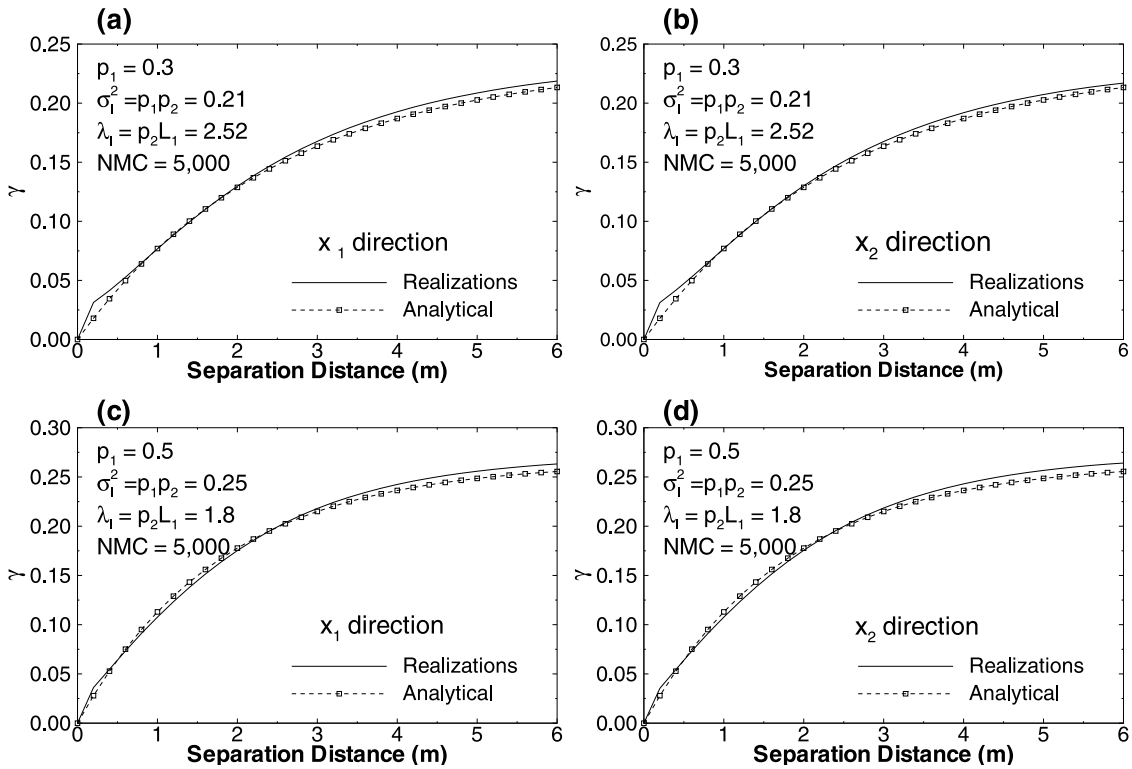

Figure 4. Comparison of variograms calculated using the analytical model and using generated Markovian realizations.

satisfy the constraints given in (35) and (36). It is worthy to note that the nearly perfect match between the sample variogram computed from Markovian random fields and the exponential variogram confirms numerically the correctness of the expression for the indicator covariance (29) with the correlation length λ_I (28).

[25] Each Markovian random field is then combined with two Gaussian continuous realizations that are scaled from zero mean and unit variance to the specified means and variances of the two categories to form a new random field Y according to

$$Y^{(i)}(\mathbf{x}) = \begin{cases} f_1^{(i)}(\mathbf{x})\sigma_{Y_1} + \langle Y_1 \rangle & \text{if } I^{(i)}(\mathbf{x}) = 0 \\ f_2^{(i)}(\mathbf{x})\sigma_{Y_2} + \langle Y_2 \rangle & \text{if } I^{(i)}(\mathbf{x}) = 1 \end{cases} \quad i = 1, 2, \ldots, 5000 \tag{38}$$

where $f_j^{(i)}$ is the ith continuous random field for the jth material, $I^{(i)}$ is the ith Markovian realization, $\langle Y_1 \rangle$ and $\langle Y_2 \rangle$

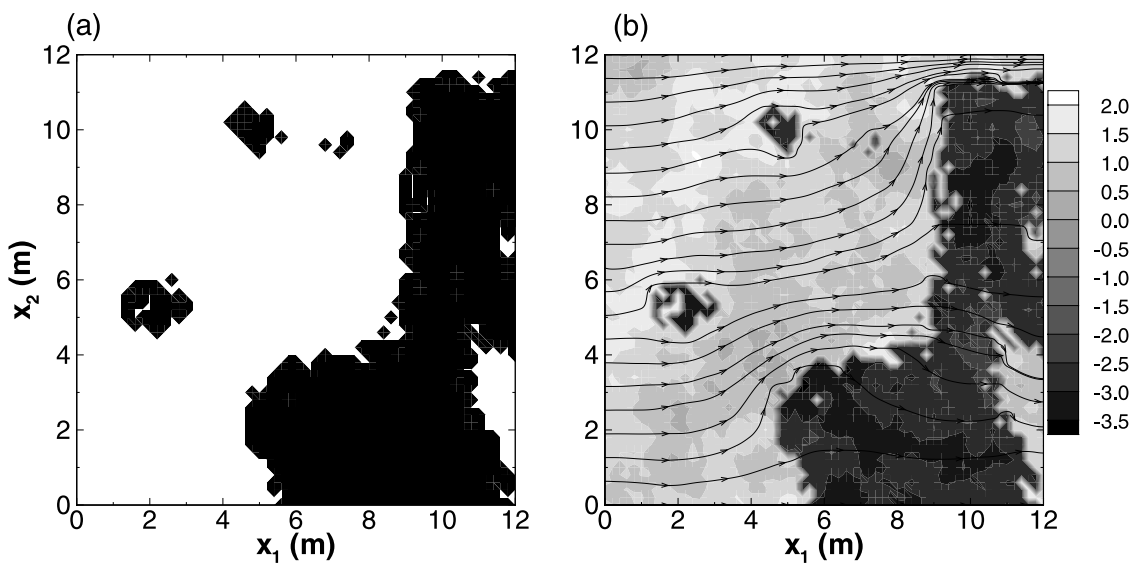

Figure 5. Examples of (a) a Markovian realization and (b) a composite log hydraulic conductivity field combined from this Markovian realization and two Gaussian realizations.

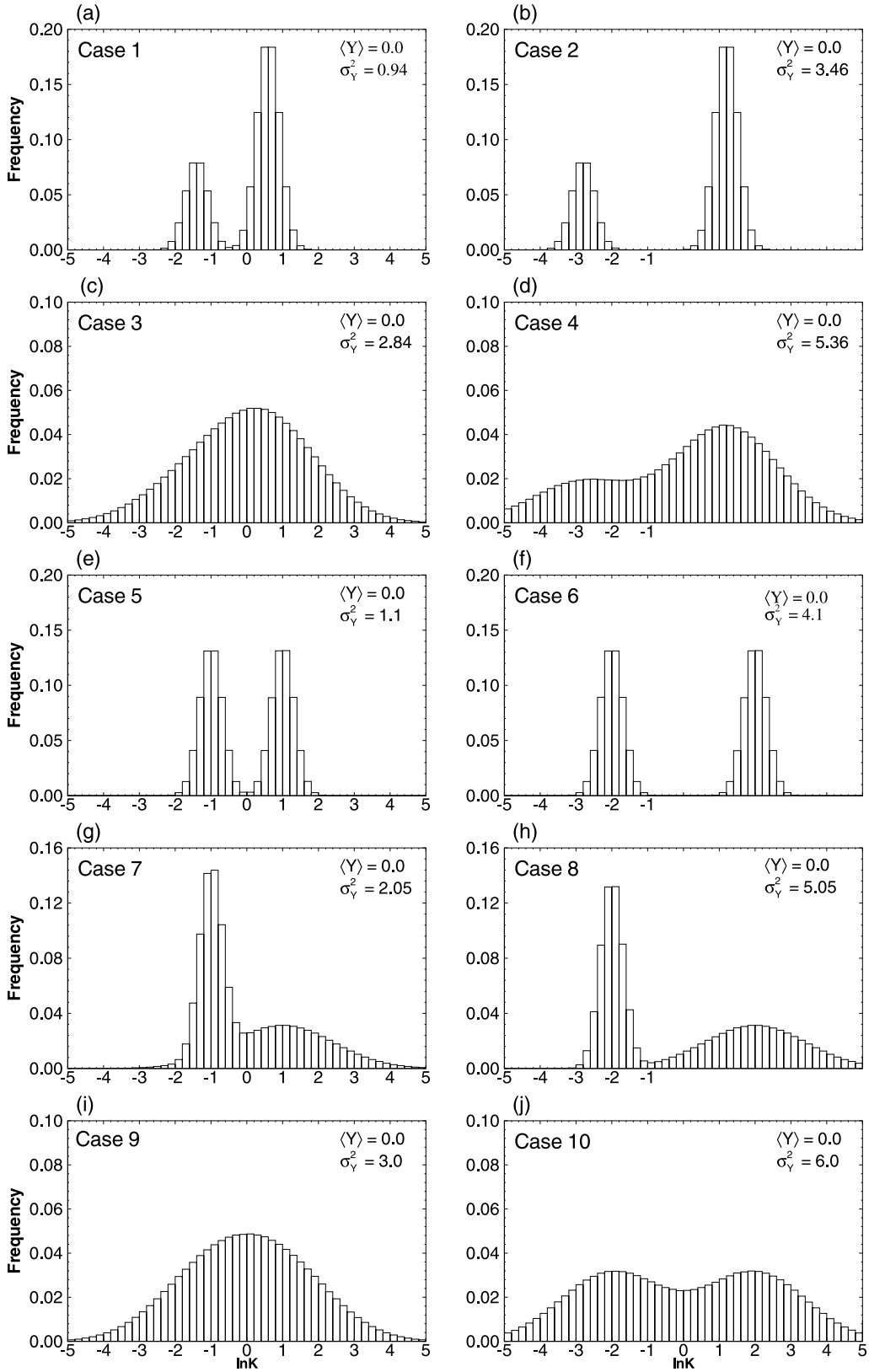

Figure 6. Histograms of the composite log hydraulic conductivity fields for numerical simulation cases 1–10.

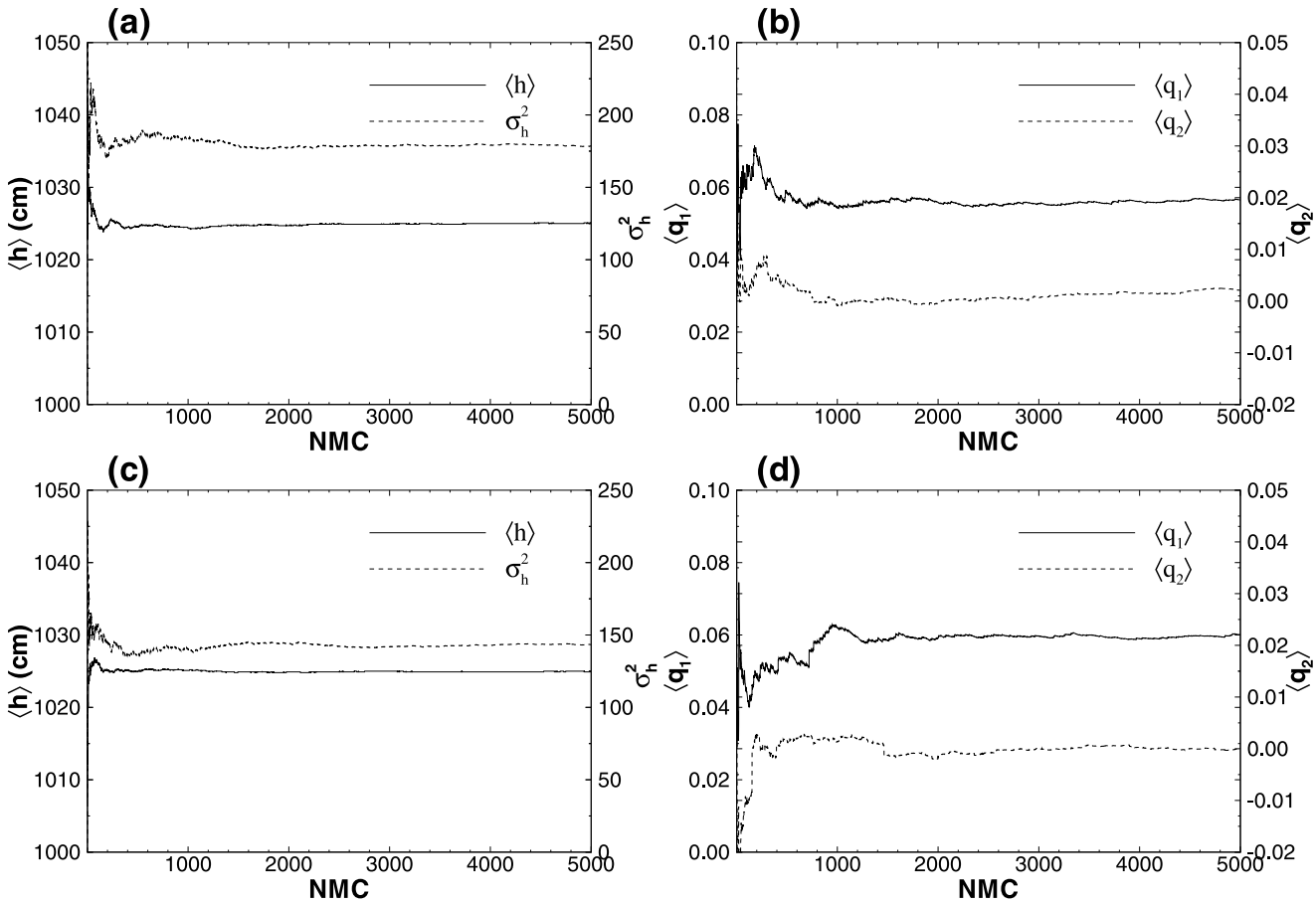

Figure 7. Convergence check for case 10 ($\sigma_Y^2 = 6.0$), (a and b) for bimodal Monte Carlo simulations and (c and d) for unimodal Monte Carlo simulations.

are the mean log hydraulic conductivities for two categories, respectively, and σ_{Y_1} and σ_{Y_2} are the standard deviations of log hydraulic conductivities for the categories, respectively. As an example, one bimodal Markovian realization with proportion $p_1 = 0.3$ and the composite bimodal realization for case 2 are shown in Figure 5, with a weighted mean $\langle Y \rangle = 0.0$ and a total variance $\sigma_Y^2 = 3.46$. The histograms of the generated log hydraulic conductivity realizations for cases 1–10 are shown in Figure 6, where each histogram is obtained from 18,605,000 (= 61 × 61 × 5,000) data points. For each realization, the saturated steady state flow equation is solved using Finite-Element Heat- and Mass- Transfer code (FEHM) developed by *Zyvoloski et al.* [1997]. The convergence of Monte Carlo simulations is checked graphically by selecting some points in the domain and plotting the ensemble statistics of head and fluxes at these points against the number of Monte Carlo simulations. Figures 7a and 7b show the ensemble behavior of mean head, head variance, and mean fluxes at the center of the flow domain for case 10 ($\sigma_Y^2 = 6.0$) as functions of the number of Monte Carlo simulations. It is seen from the Figure 7 that 5000 realizations are adequate for flow with given boundary conditions. These Monte Carlo simulation results, based on bimodal random fields, are termed "bimodal Monte Carlo simulations" and are considered the "true" solution that is the basis for comparison between different approaches.

[26] The second set of Monte Carlo simulations is done for the "equivalent" unimodal fields with exponential covariance models. For each case, we generated 5000 Gaussian continuous realizations with the mean, variance, and integral scale computed for the composite fields, as shown in the last three columns of Table 1. These Monte Carlo simulations are termed "unimodal Monte Carlo simulations." The convergence check for unimodal Monte carlo simulations of case 10 in the center of the flow domain is also shown in Figures 7c and 7d.

[27] Two more approaches are compared against bimodal and unimodal Monte Carlo simulations. By the term "bimodal moment-based approach," we mean that the second-order moment-based stochastic model [*Zhang and Winter*, 1998; *Zhang and Lu*, 2002] is applied to a statistically homogeneous field with a mean calculated from (13) and a covariance function defined in (33), which is a summation of five exponential terms (with three correlation lengths: λ_1, λ_2, and λ_I). By the term "unimodal moment-based approach," we mean that the second-order moment-based approach is applied to an "equivalent" statistically homogeneous field with the mean, variance, and integral scale as shown in the last three columns of Table 1.

[28] The difference between the bimodal (unimodal) moment-based stochastic approach and the bimodal (unimodal) Monte Carlo simulations represents the truncation error introduced by ignoring higher-order terms in the

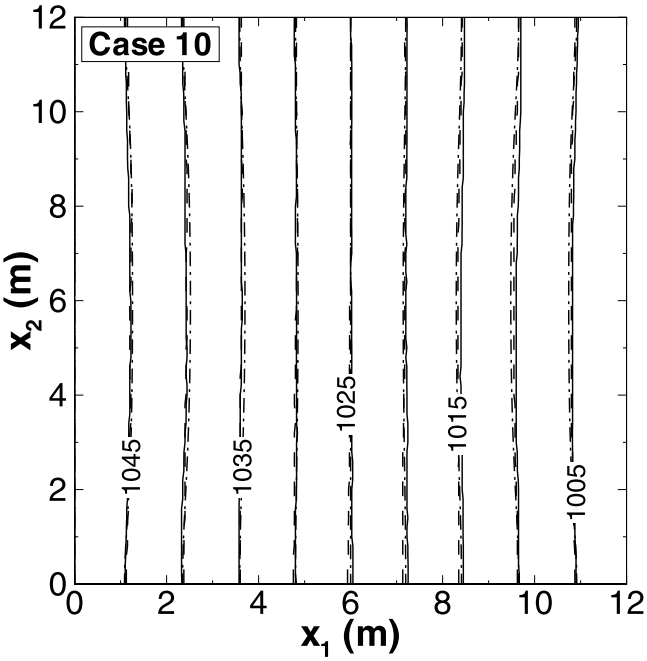

Figure 8. Comparison of the mean head field obtained from four different approaches for case 10.

moment-based approach as well as the numerical and statistical errors that occurred in Monte Carlo simulations. The difference between the two types of Monte Carlo simulations indicates how well a bimodal field is approximated by its ''equivalent'' unimodal field.

[29] The main purpose of these examples is to discuss the applicability of the moment-based approaches and the unimodal Monte Carlo simulations to flow in a bimodal porous medium. It is also of interest to see if the second-order bimodal moment-based stochastic model makes any improvement, compared to the second-order unimodal moment-based stochastic model.

6. Results and Discussion

[30] For all cases, the mean head predictions derived from the four different approaches are very close. Figure 8 shows the mean head computed from the four approaches for case 10, the case with $\sigma_Y^2 = 6.0$. However, the variance associated with the mean head predictions may differ significantly among different approaches. Figure 9 illustrates the head variance profiles along the line passing through the center of the flow domain and parallel to the x_1 direction for the four different approaches, for the cases with $p_1 = 0.3$. The solid lines in Figure 9 stand for the head variance computed from the bimodal Monte Carlo simulations (the ''true'' solution), the dashed lines stand for results from the bimodal moment-based stochastic model, the open circles stand for results from the unimodal Monte Carlo simulations, and the open squares stand for the unimodal moment-based stochastic model. Similar plots for the cases with $p_1 = 0.5$ are shown in Figure 10.

[31] A few observations can be made from Figures 9 and 10. First, when the total variance of the composite bimodal field is small (for example, $\sigma_Y^2 = 0.94$ and 1.10, for cases 1 and 5, respectively), the head variances computed from the four different approaches are very close, even though the distribution of log hydraulic conductivity is bimodal and asymmetric (case 1). This implies that in this situation both unimodal and bimodal moment-based stochastic models are applicable to flow in the bimodal porous media. For Monte

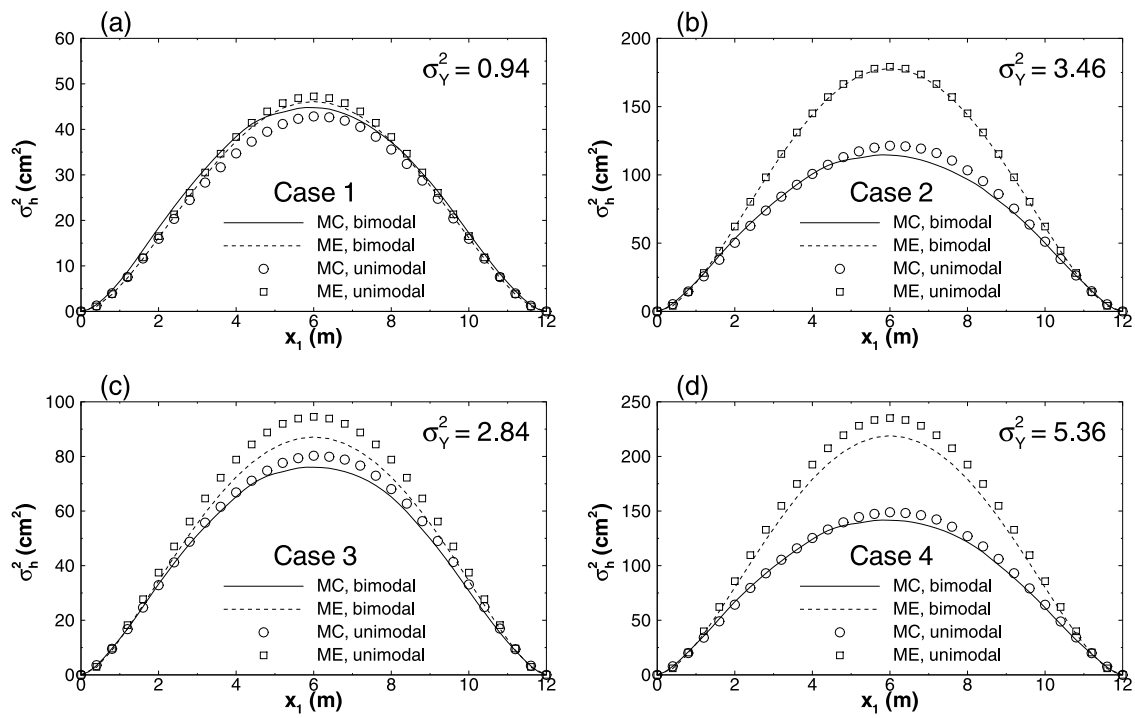

Figure 9. Comparison of the head variance obtained from four different approaches for cases 1–4 ($p_1 = 0.3$).

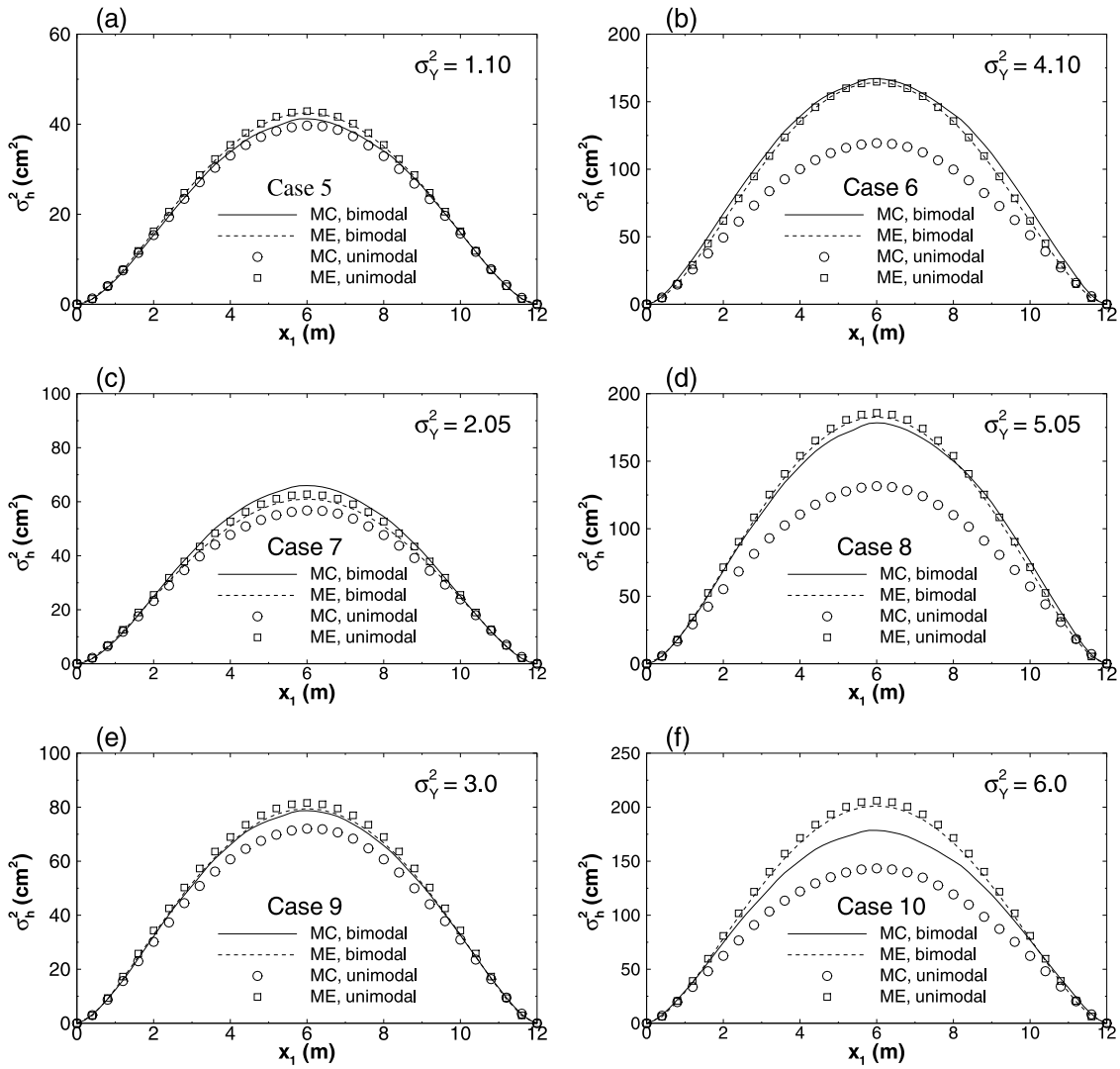

Figure 10. Comparison of the head variance obtained from four different approaches for cases 5–10 ($p_1 = 0.5$).

Carlo simulations of flow in a bimodal medium of small variability, one may either generate bimodal realizations or simply generate "equivalent" unimodal Gaussian realizations using the "equivalent" parameters.

[32] Secondly, the bimodal Monte Carlo results are very close to the unimodal Monte Carlo results in cases 1–4, but they are significantly different in cases 5–10. We have conducted a new set of simulations by a different random generator, the fast Fourier transformation by *Gutjahr* [1989], for both unimodal and bimodal Monte Carlo simulations, and have found consistent results. This indicates that the bimodal field with $p_1 = 0.3$ (i.e., 0.3–0.7 proportions) can be well represented by an equivalent unimodal field for the considered cases with a relatively small contrast between the two materials, while the bimodal field with $p_1 = 0.5$ (i.e., 0.5–0.5 proportions) may not be adequately represented by a unimodal field with "equivalent" parameters. This is understandable if one realizes that in cases 5–10, there are two distinct, equally important modes, while in cases 1–4, one of the two modes dominates. This result implies that instead of conducting bimodal Monte Carlo simulations, one may need only to perform unimodal Monte Carlo flow simulations if one material is dominant (in the volumetric fraction) in the bimodal medium and the contrast between two materials is relatively small. However, if the volumetric fractions of the two materials are close, then even for a bimodal field with a small contrast between the two materials and a small spatial variation within each material (i.e., case 6), the unimodal Monte Carlo simulation cannot substitute for the bimodal Monte Carlo simulation.

[33] Thirdly, for the cases with $p_1 = 0.3$, when σ_Y^2 is relatively large (for example, case 2), there is a large difference between the head variances obtained from the moment-based approaches and the Monte Carlo simulations, indicating that the truncation errors due to ignoring higher-order terms in the moment-based approaches are significant and that the second-order moment-based stochastic approach is not adequate. It is well documented in the literature that the unimodal moment-based stochastic model breaks down for large σ_Y^2 systems. However, for the cases with $p_1 = 0.5$, the head variances from the moment-based stochastic approaches and the bimodal Monte Carlo simulations are almost perfectly matched at $\sigma_Y^2 = 4.1$ (case 6) and

are still reasonably close even at $\sigma_Y^2 = 6.0$ (case 10). As expected for large σ_Y^2 values as in cases 6, 8, and 10, due to neglecting higher-order terms in the moment-based models, there exists a large difference between results from the unimodal moment-based stochastic model and the unimodal Monte Carlo simulations. However, for these cases there exists a close match between the moment-based stochastic model and the bimodal Monte Carlo simulations. This observation is surprising because the composite variance of log hydraulic conductivity is larger for these cases than for cases 2 and 4. Although we do not have a firm explanation for it, we suspect that this unexpectedly good match in cases 6, 8, and 10 is related to the fact that the two categories have 0.5–0.5 volumetric fractions and the variability in each category is relatively small although the composite one is large, under which circumstance the higher-order terms may be small. Being consistent with our hypothesis, the difference between the moment-based stochastic approaches and the bimodal Monte Carlo simulations increases, as the increase of spatial variability of Y_i within each material and as the increase of the composite variance σ_Y^2 (Figures 10b, 10d, and 10f) indicating that the second-order moment-based stochastic approaches become less accurate. For case 11 where the contrast in the mean log hydraulic conductivity is 6 and the variance of each material is 2.0, leading to a composite variance of $\sigma_Y^2 = 11$ (Table 1), the difference between the moment-based approaches and the Monte Carlo simulations becomes unacceptably large (Figure 11). To validate or invalidate this hypothesis, however, requires an evaluation of higher-order terms truncated in the second-order moment-based model, perhaps, on the basis of high-resolution Monte Carlo simulations.

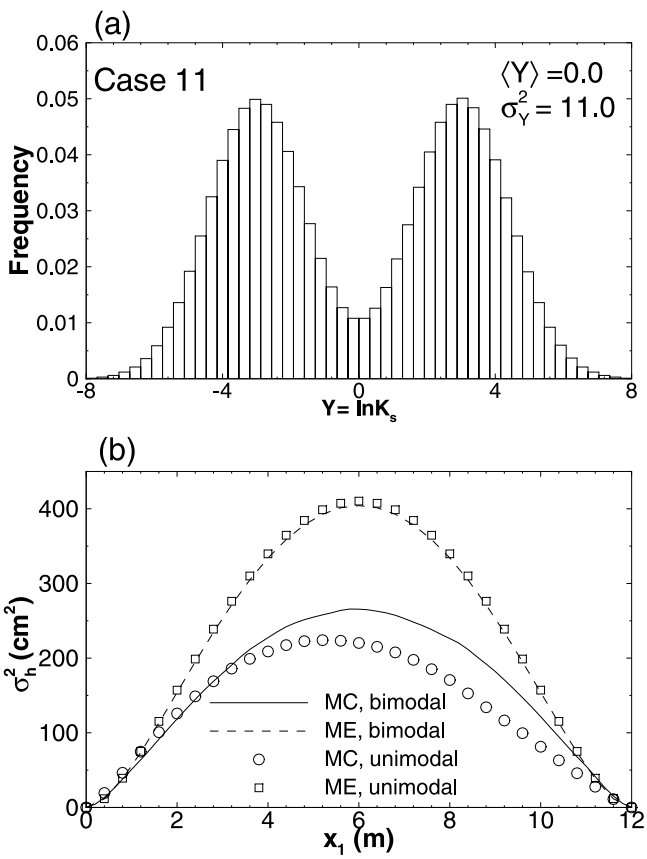

Figure 11. Histograms of the composite log hydraulic conductivity field and variances of hydraulic head for case 11 ($p_1 = 0.5$).

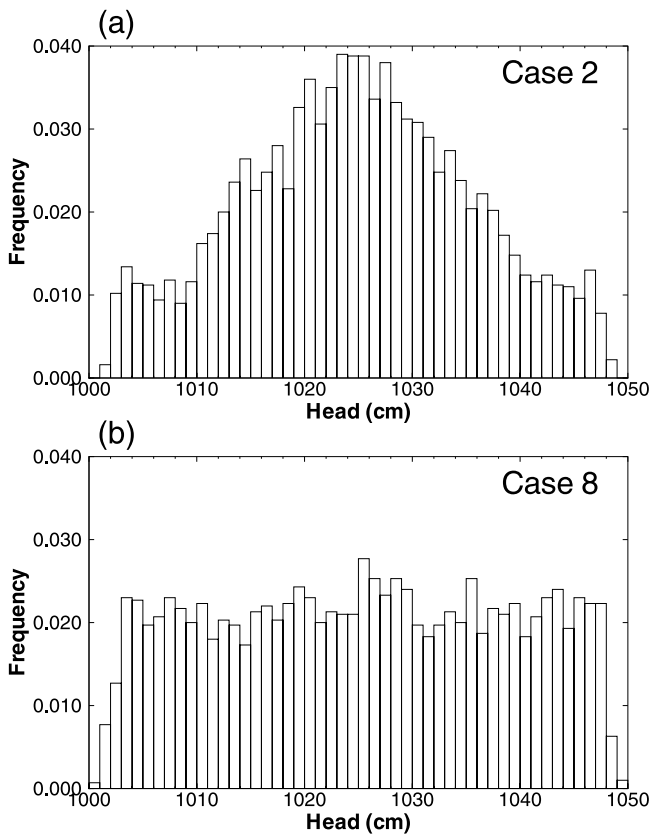

Figure 12. Histograms of the hydraulic head fields for cases 2 and 8.

[34] Fourth, comparing to those computed from the unimodal moment-based stochastic model, the head variance obtained from the bimodal moment-based stochastic model is slightly better in general (i.e., closer to the bimodal Monte Carlo simulation results), especially when the distribution of the log hydraulic conductivity is asymmetric and the total variance of Y is relatively larger (Figures 9c and 9d). When the distribution of Y has only one peak (due to a small difference in mean Y between the two materials and a large variation within each material, $\sigma_{Y_i}^2 = 2.0$), as shown in Figures 7c and 7i, the head variances from the four approaches are still close (Figures 9c and 10e), though the total variance of Y is large in these two cases ($\sigma_Y^2 = 2.84$ and 3.0, respectively).

[35] Finally, it is of interest to note that even if the composite log hydraulic conductivity field is bimodal (Figure 6), the hydraulic head field in such a domain is, in general, unimodal. This may be attributed to the elliptic nature of the governing flow equation, which regularizes the bimodal hydraulic conductivity field. Figure 12 shows the histograms of the hydraulic head at the center of the domain for cases 2 and 8. An implicit assumption with the second-order stochastic models is that only the first two moments are important and applying these models to multimodal media may thus be questionable. However, the observation in Figure 12 that the hydraulic head is not

bimodal may explain to some extent the applicability of the second-order moment-based stochastic models to bimodal (and, probably, multimodal) media.

7. Conclusions

[36] This study leads to six major conclusions.

1. The correlation lengths of the indicator random variables are functions of the statistics of materials in the multimodal porous media, and they cannot be assigned arbitrarily as done in the literature. For a porous medium with two materials, the correlation length of the indicator variable is the harmonic mean of the mean lengths of two materials, as in (28). If the mean lengths of materials are direction-dependent, so does the correlation length of the indicator random variable.

2. When the variance of the composite log hydraulic conductivity ln K_s field is small, for example $\sigma_Y^2 < 1.0$, no matter what the ln K_s distribution is, the moment-based stochastic models can be directly applied to a multimodal porous medium. For Monte Carlo simulations for flow in the multimodal porous medium, either multimodal Monte Carlo simulations or simple unimodal Monte Carlo simulations are appropriate.

3. In the case that one material is dominant (in terms of the volumetric fraction) and the total variance of the composite field is relatively high (such as cases 2 and 4), the unimodal Monte Carlo simulation with "equivalent" parameters constitutes a good approximation. Under these circumstances, truncated moment-based stochastic models suffer the same well known limitation of nominally small variance for flow in unimodal media. This limitation has been attributed to the higher-order terms truncated, which can be large. However, if none of these materials dominates, it is surprising that the results from the truncated moment-based models and from the multimodal Monte Carlo simulations are in excellent agreement for $\sigma_Y^2 = 4.1$ and in still reasonably good agreement even at $\sigma_Y^2 = 6.0$. This may imply that the higher-order terms ignored in the moment-based models are not significant for these cases. Of course, a further increase of σ_Y^2 leads to a larger difference between the truncated moment-based models and the Monte Carlo simulations, as shown in Figure 11 for case 11 ($\sigma_Y^2 = 11.0$).

4. Although in some cases the results from the moment-based model with a covariance function of multiple correlation lengths are slightly better than those from the unimodal moment-based model, they are almost the same in most of the cases examined. This suggests that either multimodal or unimodal moment-based stochastic models may be used.

5. Even if the composite log hydraulic conductivity field is multimodal, the hydraulic head field is, in general, unimodal. This may explain to some extent the applicability of the second-order moment-based stochastic models to flow in multimodal media.

6. The applicability of the second-order moment-based stochastic models to a multimodal porous medium is limited by the fact that in reality the mean log hydraulic conductivities between different materials may differ by several orders of magnitude. Thus, the total variance of the ln K_s can be very large, as in case 11 where the contrast of mean log hydraulic conductivity is 6. In the latter case, the ratio of the mean hydraulic conductivities of two materials is 403, which is not uncommon in sandstone/shale formations.

Appendix A

[37] From (23) and (24), it is clear that, for a bimodal porous medium with given proportion p_1 and one mean length, say L_1, the transition rate matrix R must be in the following format:

$$R = \begin{bmatrix} -1/L_1 & 1/L_1 \\ p_1/p_2L_1 & -p_1/p_2L_1 \end{bmatrix} \tag{A1}$$

where $p_2 = 1 - p_1$. Two eigenvalues of $\mathbf{R}$ are $\eta_1 = 0$ and $\eta_2 = -1/p_2L_1 = -1/p_1L_2 = -(L_1 + L_2)/L_1L_2$. The spectral component matrices corresponding these eigenvalues can be calculated

$$Z_1 = \prod_{m\neq 1}(\eta_m E - R)/\prod_{m\neq 1}(\eta_m - \eta_1) = \frac{\eta_2 E - R}{\eta_2 - \eta_1} = \begin{bmatrix} p_1 & p_2 \\ p_1 & p_2 \end{bmatrix} \tag{A2}$$

and

$$Z_2 = \prod_{m\neq 2}(\eta_m E - R)/\prod_{m\neq 2}(\eta_m - \eta_2) = \frac{\eta_1 E - R}{\eta_1 - \eta_2} = \begin{bmatrix} p_2 & -p_2 \\ -p_1 & p_1 \end{bmatrix}. \tag{A3}$$

Substituting (A2) and (A3) into (18), one gets

$$\mathbf{T} = (t_{ij}) = \begin{bmatrix} p_1 & p_2 \\ p_1 & p_2 \end{bmatrix} + e^{-\frac{h}{\lambda_I}} \begin{bmatrix} p_2 & -p_2 \\ -p_1 & p_1 \end{bmatrix} \tag{A4}$$

where $\lambda_I = L_1L_2/(L_1 + L_2)$ is the harmonic mean of the two mean lengths.

Appendix B

[38] For a porous medium with three different materials, (23) and (24) give five independent equations. If proportions of all three categories are known (maybe from other directions) and one mean length in the direction is known, then we are able to specify all three diagonal terms of the transition rate matrix $\mathbf{R}$. We can solve r_{ij} with one free variable and $\mathbf{R}$ has the following format:

$$\mathbf{R} = \begin{bmatrix} -\frac{1}{L_1} & \frac{1-L_3r}{L_1} & \frac{L_3r}{L_1} \\ \frac{L_3r}{L_2} & -\frac{1}{L_2} & \frac{1-L_3r}{L_2} \\ \frac{1-L_3r}{L_3} & r & -\frac{1}{L_3} \end{bmatrix} \tag{B1}$$

where r is a free variable satisfying $0 \le r \le 1/L_3$. The eigenvalues of $\mathbf{R}$ are $\eta_1 = 0$ and

$$\eta_{2,3} = -\frac{1}{2}\left(\frac{1}{L_1} + \frac{1}{L_2} + \frac{1}{L_3}\right) \pm \sqrt{\left(\frac{1}{L_1} + \frac{1}{L_2} + \frac{1}{L_3}\right)^2 - 4\frac{L_1 + L_2 + L_3}{L_1L_2L_3}\left(L_3^2r^2 - L_3r + 1\right)}. \tag{B2}$$

The spectral component matrices corresponding to these eigenvalues can be evaluated using (17)

$$\mathbf{Z}_1 = \begin{bmatrix} p_1 & p_2 & p_3 \\ p_1 & p_2 & p_3 \\ p_1 & p_2 & p_3 \end{bmatrix}$$

$$\mathbf{Z}_2 = \frac{1}{\eta_2 - \eta_3}[\eta_3(\mathbf{Z}_1 - \mathbf{E}) + \mathbf{R}] \tag{B3}$$

$$\mathbf{Z}_3 = \frac{1}{\eta_3 - \eta_2}[\eta_2(\mathbf{Z}_1 - \mathbf{E}) + \mathbf{R}],$$

and the transition probability matrix can be written as

$$\mathbf{T}(h) = \mathbf{Z}_1 + \frac{e^{\eta_2 h}}{\eta_2 - \eta_3}[\eta_3(\mathbf{Z}_1 - \mathbf{E}) + \mathbf{R}] + \frac{e^{\eta_3 h}}{\eta_3 - \eta_2}[\eta_2(\mathbf{Z}_1 - \mathbf{E}) + \mathbf{R}]. \tag{B4}$$

References

Agterberg, F. P., *Geomathematics*, 596 pp., Elsevier Sci., New York, 1974.

Carle, S. F., A transition probability-based approach to geostatistical characterization of hydrostratigraphic architecture, Ph.D. dissertation, 182 pp., Univ. of Calif., Davis, 1996.

Carle, S. F., Implementation schemes for avoiding artifact discontinuities in simulated annealing, *Math. Geol.*, *29*(2), 231–244, 1997.

Carle, S. F., and G. E. Fogg, Transition probability-based indicator geostatistics, *Math. Geol.*, *28*(4), 453–476, 1996.

Carle, S. F., and G. E. Fogg, Modeling spatial variability with one- and multi-dimensional continuous Markov chains, *Math. Geol.*, *29*(7), 891–918, 1997.

Carle, S. F., E. M. LaBolle, G. S. Weissmann, D. VanBrocklin, and G. E. Fogg, Conditional simulation of hydrofacies architecture: A transition probability/Markov approach, in *Hydrogeologic Models of Sedimentary Aquifers, SEPM Concepts in Hydrogeol. Environ. Geol.*, vol. 1, edited by O. S. Fraser and J. M. Davis, pp. 147–170, Soc. for Sediment. Geol., Tulsa, Okla., 1998.

Dacey, M. F., and W. C. Krumbein, Markovian models in stratigraphic analysis, *Math. Geol.*, *2*(2), 175–191, 1970.

Dagan, G., *Flow and Transport in Porous Formations*, 465 pp., Springer-Verlag, New York, 1989.

Desbarats, A. J., Numerical estimation of effective permeability in sand-shale formations, *Water Resour. Res.*, *23*, 273–286, 1987.

Desbarats, A. J., Macrodispersion in sand-shale sequences, *Water Resour. Res.*, *26*, 153–163, 1990.

Deutsch, C. V., and A. G. Journel, *GSLIB: Geostatistical Software Library*, 340 pp., Oxford Univ. Press, New York, 1992.

Ethier, V. G., Application of Markov analysis to the Banff Formation (Mississippian), Alberm, *Math. Geol.*, *7*(1), 47–61, 1975.

Gelhar, L. W., *Stochastic Subsurface Hydrology*, Prentice-Hall, Old Tappan, N. J., 1993.

Gingerich, P. D., Markov analysis of cyclic alluvial sediments, *J. Sediment. Petrol.*, *39*(1), 330–332, 1969.

Goovaerts, P., Comparative performance of indicator algorithms for modeling conditional probability distribution functions, *Math. Geol.*, *26*(3), 389–411, 1994.

Goovaerts, P., Stochastic simulation of categorical variables using a classification algorithm and simulated annealing, *Math. Geol.*, *28*(7), 909–921, 1996.

Gutjahr, A. L., Fast Fourier transforms for random field generation, project report for Los Alamos Grant to New Mexico Tech, *contract 4-R58-2690R*, Dep. of Math., N. M. Inst. of Mining and Technol., Socorro, 1989.

Harbaugh, J. W., and G. F. Bonham-Carter, *Computer Simulation in Geology*, 575 pp., Wiley-Interscience, New York, 1970.

Hoeksema, R. J., and P. K. Kitanidis, An application of the geostatistical approach to the inverse problem in two-dimensional groundwater modeling, *Water Resour. Res.*, *20*, 1003–1020, 1984.

Krumbein, W. C., FORTRAN IV computer program for simulation of transgression and regression with continuous-time Markov models, *Comput. Contr. 26*, 38 pp., Kansas Geol. Surv., Lawrence, 1968.

Krumbein, W. C., and M. F. Dacey, Markov chains and embedded Markov chains in geology, *Math. Geol.*, *1*(1), 79–96, 1969.

Lin, C., and J. W. Harbaugh, *Graphic Display of Two- and Three-dimensional Markov Computer Models in Geology*, 180 pp., Van Nostrand Reinhold, New York, 1984.

Miall, A. D., Markov chain analysis applied to an ancient alluvial plain succession, *Sedimentology*, *20*(3), 347–364, 1973.

Politis, D. N., Markov chains in many dimensions, *Adv. Appl. Prob.*, *26*(3), 756–774, 1994.

Ritzi, R. W., Behavior of indicator variograms and transition probabilities in relation to the variance in lengths of hydrofacies, *Water Resour. Res.*, *36*(11), 3375–3381, 2000.

Rolke, W. A., Continuous-time Markov processes as a stochastic model for sedimentation, *Math. Geol.*, *23*(3), 297–304, 1991.

Ross, S., *Introduction to Probability Models*, 5th ed., 556 pp., Academic, San Diego, Calif., 1993.

Rubin, Y., Flow and transport in bimodal heterogeneous formations, *Water Resour. Res.*, *31*, 2461–2468, 1995.

Rubin, Y., and A. G. Journel, Simulation of non-Gaussian space random functions for modeling transport in groundwater, *Water Resour. Res.*, *27*, 1711–1721, 1991.

Russo, D., J. Zaidel, and A. Laufer, Numerical analysis of flow and transport in variably saturated bimodal heterogeneous porous media, *Water Resour. Res.*, *37*, 2127–2141, 2001.

Sudicky, E. A., A natural gradient experiment on solute transport in a sand aquifer: Spatial variability of hydraulic conductivity and its role in the dispersion process, *Water Resour. Res.*, *20*, 2069–2082, 1986.

Winter, C. L., and D. M. Tartakovsky, Mean flow in composite porous media, *Geophys. Res. Lett.*, *27*, 1759–1762, 2000.

Zhang, D., *Stochastic Methods for Flow in Porous Media: Coping With Uncertainties*, 350 pp., Academic, San Diego, Calif., 2002.

Zhang, D., and Z. Lu, Stochastic analysis of flow in a heterogeneous unsaturated–saturated system, *Water Resour. Res.*, *38*(2), 1018, doi:10.1029/2001WR000515, 2002.

Zhang, D., and C. L. Winter, Nonstationary stochastic analysis of steady state flow through variably saturated, heterogeneous media, *Water Resour. Res.*, *34*, 1091–1100, 1998.

Zyvoloski, G. A., B. A. Robinson, Z. V. Dash, and L. L. Trease, Summary of the models and methods for the FEHM application—A Finite-Element Heat- and Mass-Transfer code, *LA-13307-MS*, Los Alamos Natl. Lab., 1997.

Z. Lu and D. Zhang, Hydrology, Geochemistry, and Geology Group (EES-6), Los Alamos National Laboratory, Los Alamos, New Mexico, USA. (zhiming@lanl.gov)